Astron. Astrophys. 340, 569–578 (1998)

ASTRONOMY
AND
ASTROPHYSICS

TESOS, a double Fabry-Perot instrument for solar spectroscopy

T.J. Kentischer, W. Schmidt, M. Sigwarth, and M.v. Uexküll

Kiepenheuer Institut für Sonnenphysik, Schöneckstrasse 6, D-79104 Freiburg, Germany (e-mail: tk; wolfgang; msig; uex@kis.uni-freiburg.de)

Received 27 March 1998 / Accepted 31 July 1998

Abstract. A double Fabry-Perot spectrometer in a telecentric configuration (TESOS: Telecentric Etalon SOlar Spectrometer) has been developed and installed in the Vacuum Tower Telescope at the Observatorio del Teide, Tenerife. The control system allows to switch from one wavelength band to another within 2 seconds. The telecentric configuration provides a constant wavelength passband across the field of view. Servo-stabilized etalons and a stable thermal environment provide a wavelength stability of <0.3 picometer per hour. We present initial results obtained with this instrument.

Key words: Sun: particle emission – Sun: magnetic fields – instrumentation: spectrographs – instrumentation: interferometers

1. Introduction

The observational study of the dynamics of solar small-scale structures is of high astrophysical interest, and the quality of the measurements has mostly been limited by the instrumentation. This motivated us to complement the focal plane instruments of our telescope with a newly designed filter spectrograph. The key characteristics were chosen to optimize the instrument for the investigation of magnetic elements and sunspot dynamics and magnetism, as well as for observations of chromospheric waves and their relationship to the photosphere. In the case of the sunspots a field of view of more than 60 arcsec is important to include the spot and the surrounding moat in the velocity and magnetic field measurements. This allows to treat e.g. the important question of mass conservation of the penumbral flow. (Westendorp-Plaza et al., 1997, Schlichenmaier et al., 1998, Schmidt, 1998). Chromospheric observations require a field of view that covers several supergranulation cells. In both cases oscillation and waves with periods down to 180 s are involved, chromospheric grains have even shorter characteristic time scales of about 100 s (v. Uexküll & Kneer, 1995). The investigation of these phenomena therefore requires high temporal resolution. On the other hand one needs sufficiently long sequences to achieve the necessary frequency resolution for the study of oscillatory phenomena. Long-term stability of the instrument is essential for this kind of measurements. Furthermore it is very desirable to perform simultaneous or nearly simultaneous measurements in different wavelength regions in order to cover some height range in the solar atmosphere. This was indeed one of the main drivers for the design of a new instrument.

Spectroscopy is the backbone of observational solar physics, it provides the relevant information for a proper understanding of physical processes in the solar atmosphere. Unlike broadband imaging, spectroscopic measurements are always photon-starved, especially when observations near the resolution limit of the telescope are concerned. Classical grating spectrographs enjoy very high spectral resolution, better than 1 picometer, or $\lambda/\delta\lambda = 800.000$. On the other hand, their intrinsic field of view is limited by the length and width of the spectrograph slit, the latter being less than about an arcsecond to match the telescope's resolution. Covering a reasonably sized field of view at fixed wavelength requires scanning of the solar images across the slit, a time consuming procedure which also deteriorates the effective resolution due to changing atmospheric seeing.

A 2-dimensional filter spectrograph with a 2D detector array circumvents the problem of spatial scanning and its field of view is rather large: one to two arcminutes, depending on the instrument characteristics. However, the large field of view has to be paid for: now the wavelength information is obtained by scanning through the spectral region of interest. But this scanning procedure takes typically only 10 – 20 steps, and it is rather straightforward to combine the individual narrowband filtergrams to a full 2D-spectrogram.

The main objectives are summarized in the following section. Sect. 3 deals with some important considerations about FPIs. A detailed description of the instrument and its operational aspects is given in Sect. 4. The instrument performance and "first light" results are presented in Sect. 5.

2. Objectives

Only a few spectrometers based on two or more Fabry-Perot etalons have been built and successfully used in astrophysical applications. Very early approaches were made by Gehrke and Von Baeyer (1906) and Houston (1927). In the sixties several systems have been built, e.g. the PEPSIOS-type spectrometers (Mack et al. (1963), McNutt (1965), Stoner (1966), Ramsay et

al. (1970)) and the triple FPI system of the Culgoora Observatory (Loughhead et al. 1978). Darvann and Owner-Petersen (1994) carried out a thorough study of a possible FPI-filter for the LEST telescope. Very recently, the two-dimensional spectrometer of the Göttingen group (Bendlin et al. 1992) at the VTT on Tenerife has been upgraded to a double FPI system from a combination FPI – universal birefringent filter. In addition to the scientific objectives mentioned in the introduction there were a few more technical requirements that entered into the instrument design. In order to keep setup time to a minimum, reasonable effort was spent to simplify necessary setup work and to automate it wherever possible. In order to minimize environmental influence TESOS was designed as a very compact instrument in a closed housing. All movable components are motorized to reduce disturbances by opening the instrument box. The basic requirements for TESOS were:

- Wavelength range: 450–750 nm
- Field of view (FOV): $\geq$ 100 arc-sec
- Spatial pixel resolution: 0.15 arc-sec/pixel
- Spectral resolution: $\geq$ 250.000 (@500 nm)
- Frame rate: 3–5 frames/sec
- Simultaneous measurement of filtergrams and continuum frames
- Optional Stokes-V measurements
- Fast prefilter change
- Wavelength stability: $\leq$ 0.5 pm/h
- Thermal stability
- Convenient user interface
- Dual etalon system, with upgrade possibility to three etalons

Some of the above numbers are not independent of each other, and trade-offs had to be made between e.g. field of view and spectral resolution.

3. Interferometer specification

The most important issues of a multi-FPI spectrometer are the spacing ratios of the FPIs and the optical configuration, i.e. a collimated or a telecentric mount. The following two subsections describe the respective considerations and the solution adopted. The design goal was a dual FPI system, with the option to upgrade to a triple system. For TESOS we used two Queensgate ET-50 etalons with a clear aperture of 50 mm each. The etalons are coated for a wavelength range between 450 and 700 nm, with mean reflectivity of 94%. The surface quality is $\lambda/200$ before coating. Both etalons are driven by CS100 Controllers which stabilize the spacing and the parallelism via capacitance micrometers and piezo actuators. The servos operate in closed loop, eliminating non-linearity and hysteresis of the piezos.

3.1. Spacing ratios

The transmitted intensity for a single FPI as a function of the phase delay ψ between the plates is described by the Airy function

$$I(\psi) = \frac{T^2}{(1-R)^2(1+F\sin^2(\psi/2))} \quad I_0 \tag{1}$$

where R is the surface reflectivity, T the surface transmission and the coefficient F given by $F = 4R/(1-R)^2$. The phase difference ψ is given by

$$\psi = 4\pi d\mu\cos\theta/\lambda \tag{2}$$

(In our case: μ=1, i.e. air between the plates). d is the plate separation, θ the angle of incidence and λ the wavelength. This leads to the typical transmission pattern with maxima of the order n, $n = 1, 2, ...$ for $\psi = 2\pi n$ and a free spectral range FSR, i.e. the spacing of two adjacent maxima, of FSR $= \lambda^2/2\mu d$. For large F the FWHM of a transmission peak $\delta\psi$ is given by

$$\delta\psi = 2(1-R)/\sqrt{R} = 2/\sqrt{F} \tag{3}$$

For the spectral resolution Res of a single FPI one obtains

$$Res = \frac{\lambda}{\delta\lambda} = \frac{\psi}{\delta\psi} = \sqrt{F}\frac{\mu d}{\lambda}\cos\theta = Fi\frac{2\mu d}{\lambda}\cos\theta \tag{4}$$

with the finesse Fi, defined as the ratio FSR/$\delta\psi$ and commonly used to characterize the resolving power of etalons. Eqs. (3) and (4) are valid only for ideal etalon plates and pointlike sources. For details on the modification of the instrumental function and transmission line-width see e.g. Vaughan 1989.
Taking into account possible transmission peak broadening mechanism like imperfect reflectivity and plate shapes, a value of 30 - 40 for the finesse is reached.

A combination of two (or more) etalons with different plate separations is used to enlarge the FSR. The resulting Airy function for a combined system is obtained by multiplying the individual functions. Near the common (or main) transmission peak at λ_0, the transmission function can be approximated by a Lorentz function T_L of the phase deviation $\Delta\psi$ from the common peak:

$$\begin{aligned} T_L(\Delta\psi) &= \frac{T_F(\Delta\psi_c)}{[1+F(1+\epsilon_2^2+\epsilon_3^2)\Delta\psi^2]} \\ \Delta\psi &= \frac{2\pi}{\lambda_0^2}d_1(\lambda-\lambda_0)\ ;\ \Delta\psi_c = \frac{2\pi}{\lambda_0^2}d_1(\lambda_c-\lambda_0) \\ \epsilon_2 &= d_2/d_1\ ;\ \epsilon_3 = d_3/d_1 \end{aligned} \tag{5}$$

T_F is the prefilter transmittance and $\Delta\psi_c$ a phase difference describing the detuning of the prefilter transmission peak with respect to the common FPI peak at λ_0; d_1 to d_3 denote the plate separations, ϵ_2 and ϵ_3 the spacing ratios of the etalon combination. (For details see Darvann & Owner-Petersen 1994). The spectral resolution for spacing ratios around 1 (Vernier ratio) is then given by

$$Res = \pi\sqrt{F(1+\epsilon_2^2+\epsilon_3^2)}\frac{d_1}{\lambda_0} \tag{6}$$

The resulting resolution is somewhat better than for larger spacing ratios, where the resolution is determined by the largest plate separation. However, for Vernier ratios one has to take more care of side lobes (ghosts) within the passband (see below).

For the largest plate separation we chose a value of 1.3 mm leading to a FSR of 0.1 nm (@500 nm). Together with a finesse of 40, we obtain a spectral resolution of at least 200.000. We

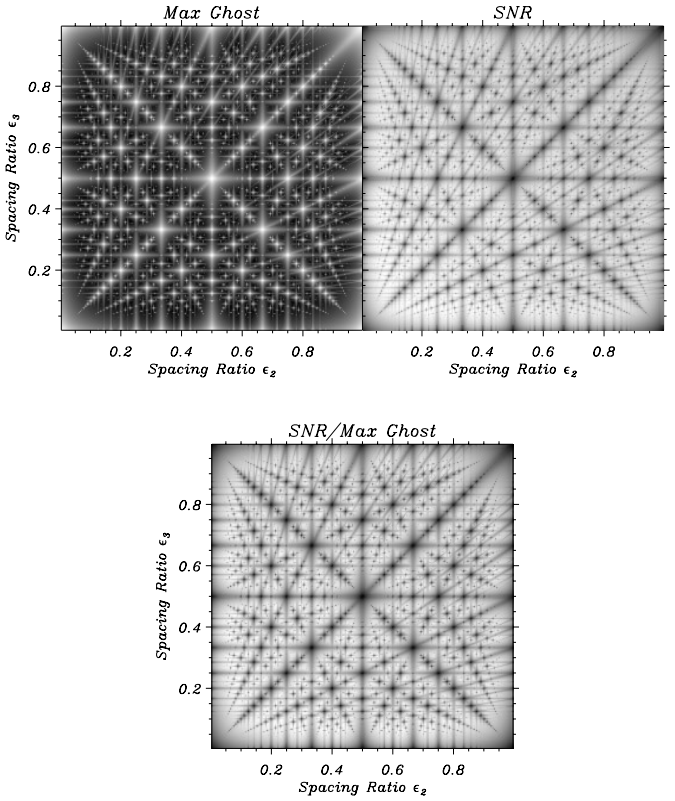

Fig. 1. Max Ghost, SNR and SNR/Max Ghost for a triple FPI system with a 1 nm FHWM interference prefilter. Large values are bright, small values dark. The plate separation of the first FPI is d_1=1.3 mm. ϵ_2 is the spacing ratio d_2/d_1 for the second, ϵ_3 the spacing ratio d_3/d_1 for the third interferometer. The computation is made for a wavelength of 400 nm.

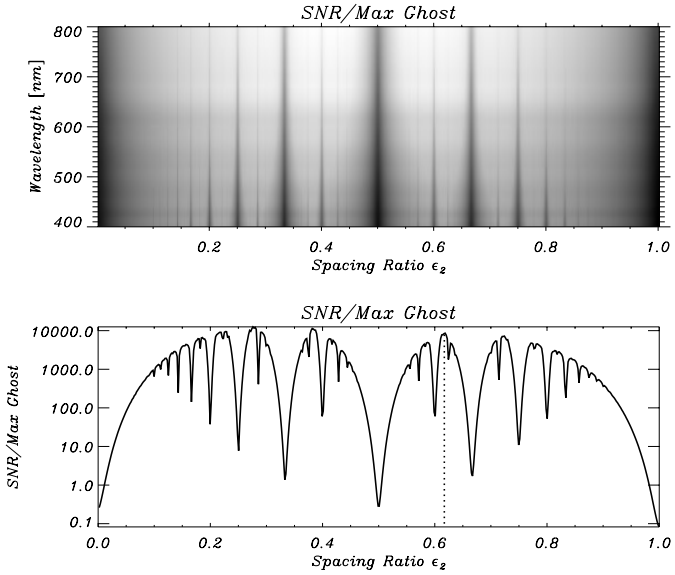

Fig. 2. SNR/Max Ghost for a tandem FPI system with a 0.3 nm FHWM interference prefilter. Large values are bright, small values dark. The plate separation of the first FPI is d_1=1.3 mm. ϵ_2 is the spacing ratio d_2/d_1 for the second etalon. The line plot corresponds to a wavelength of 400 nm. The ϵ_2 chosen for TESOS is indicated by a dotted line.

Table 1. FPI spacing ratios of TESOS. FWHM(PF) is the required width of the interference prefilters.

FPI#	ϵ	d [mm]	FWHM(PF) [nm]
1	1	1.300	
2	0.617	0.802	0.3
3	0.439	0.571	1.0

calculated the Vernier spacing ratios of a dual and a triple system using the method described by Darvann and Owner-Petersen (1994). The criteria to optimize the spacing ratios are:

– **Max Ghost** is the transmission amplitude of the strongest off band peak (ghost) of the combined FPI/prefilter system.
– Stray light signal-to-noise ratio **SNR** is the ratio of integrated light from the main transmission peak of the system to the integrated light from all side lobes within the whole spectral range

Both parameters were combined to the single performance characterization value **SNR/Max Ghost**. Figs. 1 and 2 show examples for the calculation of a triple and a double FPI-system using a 1 nm FWHM prefilter for the triple system and a 0.3 nm FWHM prefilter for the double system. The complexity of the pattern decreases for increasing wavelength. A good solution at the blue end of our wavelength range therefore holds for all larger wavelengths. In the lower panel of Fig. 1 the brightest areas indicate good choices for the spacing ratios. To decide for the best spacing ratio within the variety of good combinations, we added three criteria:

– Maximize the ratio SNR/Max Ghost for a slightly decentered prefilter passband,
– Find a combination that works both for a double system and a possible upgrade of this combination to a triple system,
– Optimize the spectral resolution for a double FPI system.

The first criterion is important, because any decentering of the prefilter causes a small change in the SNR/MaxGhost pattern. The FWHM of the prefilters for a double system is only 0.3 nm and even slight variations of the ambient temperature cause a passband shift. Fig. 2 is the equivalent to Fig. 1 for a double system. The value chosen for the double system is indicated in the Figure. The spacing ratios for a future upgrade of TESOS to a triple system are summarized in Table 1.

3.2. Optical configuration

There are essentially two optical mounting possibilities which can be adopted for the design of an FPI spectrometer:

• Collimated (classical) mounting

The FPIs are mounted near the image of the entrance pupil of the telescope (Fig. 3). Every image point corresponds to rays with a specific angle with respect to the optical axis propagating through the FPIs. The effective plate separation is a function of this angle, which results in a wavelength gradient across the

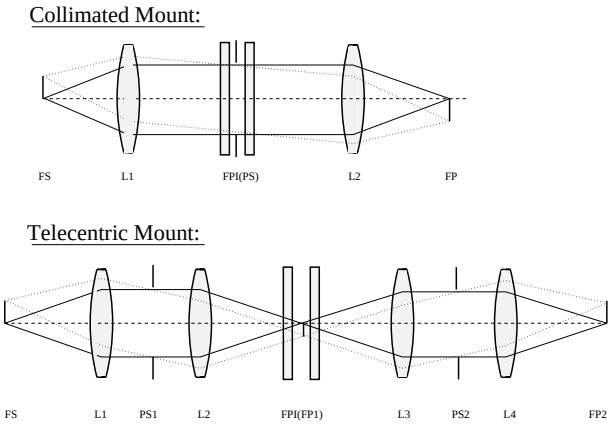

Fig. 3. Mounting concepts for FPI interferometers. In the collimated mounting, the telescope aperture (PS) is imaged into the interferometer(s), L2 is the reimaging lens. At the FPI location the beam is collimated. In the telecentric configuration, lenses L1 and L2 project the solar image (FS) into the interferometer. Lenses L3 and L4 image the solar image onto the detector (FP2).

Table 2. Comparison between collimated and telecentric interferometer mount.

	Collimated	Telecentric
Broadening mechanisms	reflectivity plate shape	reflectivity f-number
Wavelength shift across FOV	yes	no
Wavefront distortion	large	low
Influence of Dust on the image	low	large
Alignment sensitivity	large	low
Blocking Ghost reflections	difficult	easy
Influence of plate shape	broadening	λ-shift

field of view (FOV). With respect to the center of the FOV, the wavelength of the transmission maximum near the edges will be blue-shifted.

Moreover, all rays distributed across the pupil image (and the interferometer plates) with equal inclination will form one image point. Therefore non-uniformity of the plate surfaces or parallelism errors will result in a broadening of the transmitted spectral profile. So the spectral resolution is not only given by the reflection of the interferometer coatings but also by the flatness and parallelism of the plates.

• Telecentric mounting

In the telecentric configuration the pupil image is collimated and the FPIs are located near the image plane. Additional optical components reimage the sun to the camera. At the location of the etalon(s) the beams which form the image have the same cone angle at each point across the field of view. The maximum ray angle within this cone is a function of the f-number of the telecentric optics (L1 & L2 in Fig. 3, which determines the FOV together with a given clear diameter of the FPI. To attain the calculated spectral resolution of the system, the angle of this ray cone has to be minimized.

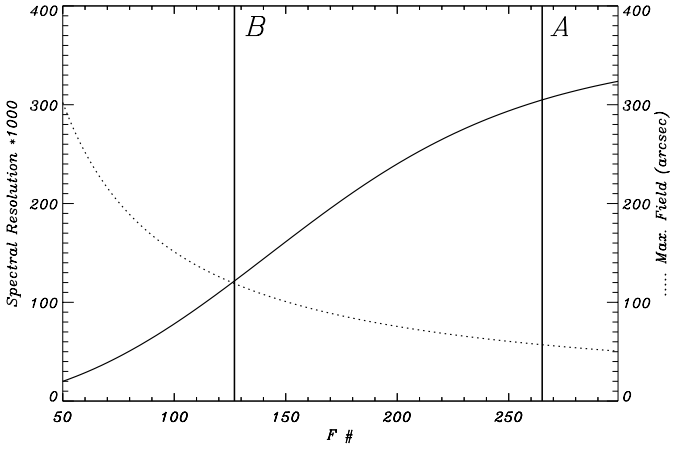

Fig. 4. Resolution of an FPI in telecentric configuration as a function of the f-ratio. The dashed curve indicates the usable FOV for a 50 mm FPI. A and B mark the two fields of view used for TESOS.

Since every position on the interferometer belongs to exactly one point within the solar image, there are no systematic wavelength shifts over the FOV due to angle variations. The spectral resolution is given by the plate reflectivity and the f-number of the optical system (Fig. 4).

To avoid image contamination due to dust on the interferometer plates or due to inhomogeneities within the coatings, the FPIs are shifted slightly away from the focal plane. Light from one image point now covers a small area (1 mm diameter) on the interferometer plates causing a small broadening of the transmitted profile due to small scale variations of the FPI-spacing (micro roughness). Large-scale variations of the plate shape or parallelism errors lead to small shifts of the transmission profile over the FOV. But these variations are usually much smaller than the wavelength dependence of the collimated mounting. The telecentric mounting allows (and requires) to trade spectral resolution against FOV. TESOS was built with two fields of view with different spectral resolution(Fig. 4):

– A: FOV: 50 arcsec; spectral resolution 320.000,
– B: FOV: 100 arcsec; spectral resolution 160.000.

The resolution numbers above refer to a wavelength of 500 nm. The reimaging optics following the interferometer set, provides a simple means to blocking ghost images by an aperture stop. In Table 2 we summarize the advantages and disadvantages of the two mounting concepts. Although collimated mounting offers a higher spectral resolution, we preferred the telecentric solution for TESOS. Collimated mounting suffers from the risk of deteriorating the image quality (Darvann & Owner-Peterson 1994).

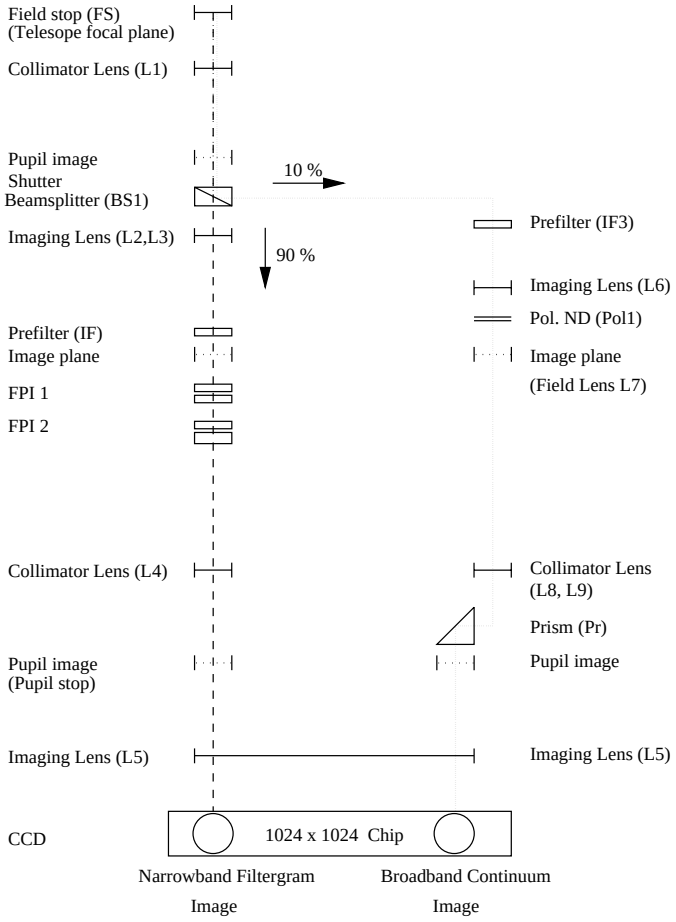

Fig. 5. Optical scheme of TESOS. Lettering is the same as in Fig. 6.

4. Spectrometer design

The optical scheme of TESOS is shown in Fig. 5. Only the main optical train and the basic elements are shown. The lettering used corresponds to that in Fig. 6. An exploded view of the mechanical layout including all calibration elements and optional features is given in Fig. 6. The telescope forms an image at the field stop (**IP0**). The sensor of the IAC/KIS Correlation Tracker(**CT**) is located near the telescope's main focus (Schmidt & Kentischer 1995).

The field stop contains four apertures: FOV 50 arcsec, FOV 100 arcsec, a target for alignment, focus adjustment and scale factor measurements and a pinhole for alignment purposes.

Lens **L1** collimates the light and forms an image of the telescope entrance aperture at the **shutter**. An intermediate image near the FPIs is formed by **L2** (**L3** for the small field of view). Etalon **FPI1** and the pre-filter wheel **PF** are mounted on a motorized rotating stage. **FPI1** together with the filter wheel are moved to different positions depending on the FOV chosen. The second interferometer **FPI2** remains fixed. The solar image is located in between **FPI1** and the prefilter wheel **PF**. The reimaging lenses **L4** and **L5** form the final image at the CCD camera. **L5** is mounted on a motorized stage to adjust for chromatic focus shifts. For the white-light reference image, 10% of the light is extracted by the beam splitter **BS1**. A set of lenses (**L6** to **L9**) forms an image and an exchangeable broadband interference filter **IF2** allows to choose a convenient spectral band for that image. The white-light image is formed next to the filter image on the camera. The filter and white-light images have the same shutter and are using the same CCD, which guarantees strict simultaneity. The intensity of the white-light channel is adjusted using two crossed polarisators (**POL1**). TESOS can be equipped with a polarization optics located behind mirror **U5**. In that configuration the light passes through a super-achromatic quarter wave plate (**Lambda/4**) and is split by a Wollaston prism **Wol**). In this case the camera records two Stokes-V circular polarized filtergrams and one white-light image (Fig. 7). Internal polarization within TESOS is minimized by two sagittal 45^o reflections followed by two tangential 45^o reflections. For monitoring purposes beam splitter **BS2** feeds 10% of the light to a video camera. To adjust the band-passes of the two FPIs on each other, the folding mirror **U5** is removed and the etalon plates are reimaged onto a photomultiplier via **L15**. A **HeNe laser** is used to adjust the parallelism of the FPIs. The light from a HeNe laser, followed by a beam expander (**L13, PH, L14**) is fed to the etalons either by **U1** or by **U2** depending on the FOV used. Both FPIs are mounted onto motorized stages, so they can be adjusted separately. The second CCD camera shown in Fig. 6 together with the folding mirror (**U10**), imaging lens (**L16**) and a diversity sensor(**PD15**) (Tritschler et al. 1997) are an auxiliary feature of TESOS for image reconstruction purposes.

4.1. Interference filters

TESOS in its present tandem configuration requires narrowband interference filters with an FWHM of 0.3 nm. The filters are mounted telecentrically just in front of the first FPI. In this position it is possible to tilt the filter in order to adjust the wavelength passband. If the interference filter is located in a pupil image, any tilt would result in a field-dependent shift of the passband This problem had been discussed e.g. by Atherton, Taylor et al. (1982) in relation with their Fabry-Perot spectrograph TAURUS. With a four position filter wheel one can easily switch between several spectral lines in a very short time (typical 1-2 seconds). We use Andover filters with a 2-cavity design, an FWHM of 0.3 nm and a typical transmission of 25%. The manufacturer guarantees the specified center wavelength to $\pm$ 0.1 nm. Each filter can be slightly tilted with a motorized mechanism within the filter wheel, to fine-tune the passband to the precise wavelength of the chosen spectral line. The tilt range of 2° corresponds to a passband shift of +0/-0.2 nm (only blue-shift is possible).

4.2. Ghost images

Back reflections of the light between the two FPIs and the interference filter lead to ghost images. The integrated intensity of such ghost images is 12% of the main passband intensity for the first reflection and 5% for the second one. By tilting the interferometers by a small angle, this parasitic light is reimaged in the pupil plane, separated from the ordinary pupil and then baffled.

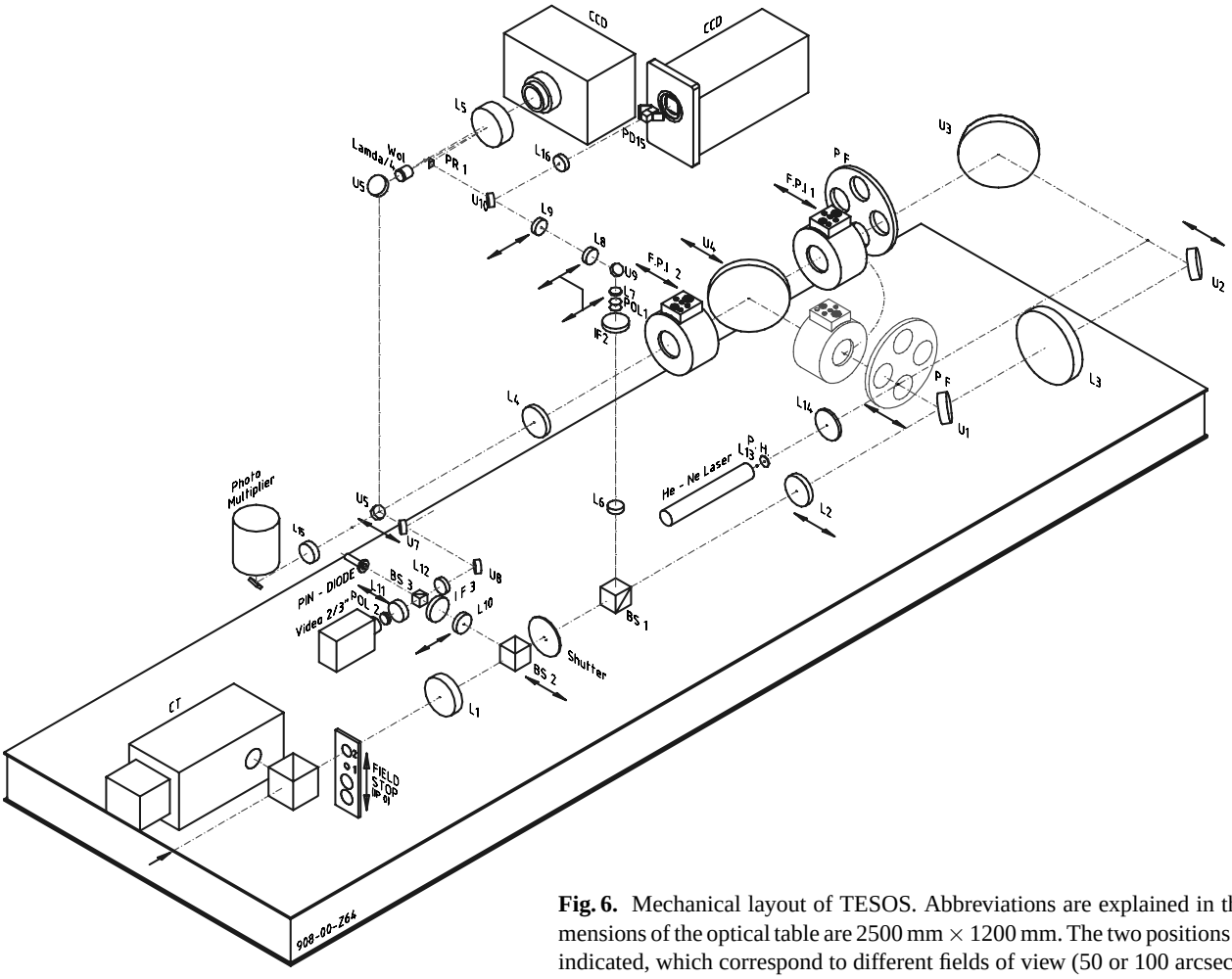

Fig. 6. Mechanical layout of TESOS. Abbreviations are explained in the text. Dimensions of the optical table are 2500 mm $\times$ 1200 mm. The two positions of FPI1 are indicated, which correspond to different fields of view (50 or 100 arcsec diameter).

The tilt angles for each interferometer are $\pm 0.05^o/\pm 0.1^o$ for the case of the 50/100 arcsec fields of view. Tilting the etalons introduces slight intensity gradients within the pupil image in one direction caused by a slight shift of the two FPI passbands.

4.3. Detector

In polarimetric mode, three different frames are simultaneously imaged on the CCD: Two Stokes-V circular polarized filtergram images and one white-light reference image (Fig. 7). If TESOS is operating in default mode, two images are on the camera and it is sufficient to read out only one half of the chip. The camera used in TESOS is part of a joint project between the Kiepenheuer-Institut and the National Solar Observatory (NSO), Sunspot, New Mexico. It consists of a Thomson TH79KA95 evaluation kit, an EDT-SDV digital video interface and a double processor SUN SPARC20 workstation (see Fig. 9). The software development of the camera driver was done at NSO.

The camera chip has 1024×1024 pixels with a pixel size of 19 μm and a digital resolution of 10 bit. The pixel scale is 0.15 arcsec/pixel within the 50 arcsec field and 0.3 arcsec/pixel in the 100 arcsec field. The readout time for a full frame is 300 msec. Writing to disk needs another 200 – 300 msec, depending on the storage media used (Exabyte, Hard Disk or Magneto-optical disk).

4.4. Photon statistics

The signal-to-noise ratio is calculated using the relevant solar data, the transmission figures for the telescope and the instrument. Fig. 8 displays the integration time of the CCD as a function of wavelength for different signal-to noise ratios (SNR) and for the different fields of view available. The parameters used for the computation are listed in Table 3. The SNR curves refer to the spectral continuum. In the cores of strong lines the intensity may be more than ten times lower, requiring longer integration times for a given SNR.

4.5. Spectrometer control

TESOS is controlled by a double processor SUN SPARC 20 workstation. The user operates the whole system via a graphical user interface (written in C, libsx) without manual manipulations inside the instrument. Fig. 9 shows a sketch of the control system. All moving parts within the instrument are motorized. The DC drives, the laser, PIN-diode and photomultiplier (PM)

Table 3. Transmission values used for the SNR-computations.

Description	T	Comment
Telescope	0.56	Al-coated mirrors, 3 windows
Correlation Tracker	0.68	Ag-coated mirrors
TESOS	0.52	excl. etalons and prefilter
Etalons	0.81	.9 each
Prefilter	0.39	peak transmission
QE of CCD	> 0.2	wavelength-dependent

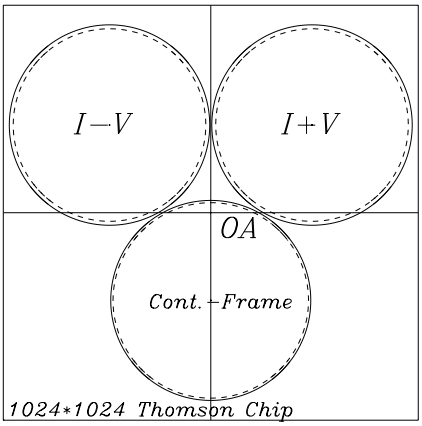

Fig. 7. CCD chip illumination in the polarimeter mode of TESOS. The optical axis (OA) is in the chip center.

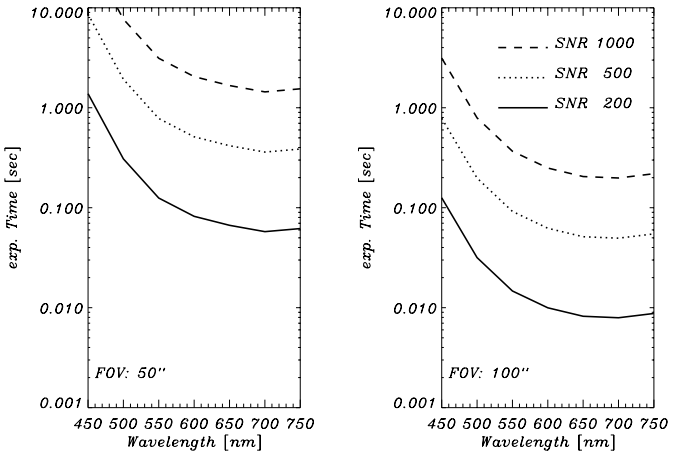

Fig. 8. Exposure time as a function of wavelength for different signal-to-noise ratios. The left (right) panel corresponds to the small (large) field of view.

are connected via a CAN-BUS (Etschberger 1994) to the workstation. Most of the necessary tasks for the etalon adjustment and observing setup are working automatically or interactively. In particular, the following procedures are (more or less) automatic:

- Setting parallelism of the FPIs.
- Locking both FPIs on a solar line.
- Centering of the prefilter passband.
- Performing flat-field and dark sequences.

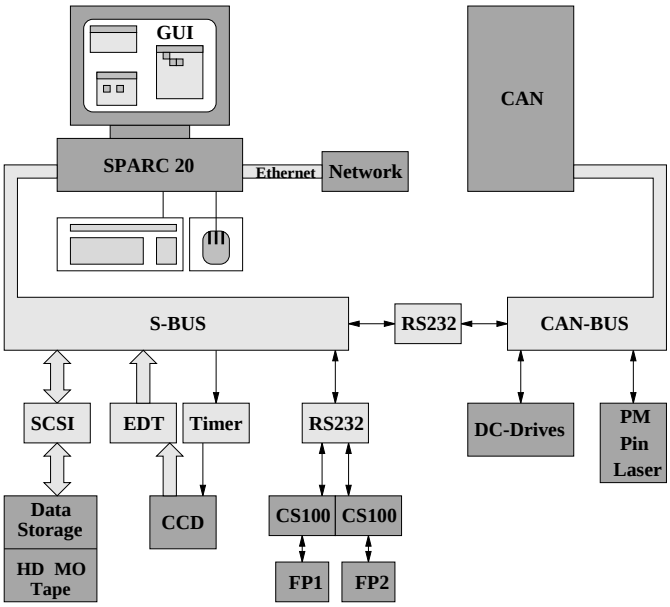

Fig. 9. Scheme of the TESOS remote control system. All devices are controlled by a SUN SPARC 20 workstation and are operated via a graphical user interface.

Complete observing setups can be saved for later use, including all motor positions, camera settings and etalon parameters.

The TESOS workstation is part of a local network and also connected to the outside world. Remote control from other workstations allows and greatly simplifies support and troubleshooting from outside the telescope site. Ethernet connections are used to interact with other instruments, e.g. the correlation tracker.

5. First measurements

TESOS was installed at the VTT in November 1996. During a few short commissioning campaigns in 1997 the hard- and software configuration were improved. First regular observations were made in late autumn of 1997.

5.1. Stability

TESOS is installed in an air-conditioned laboratory with an ambient temperature of 19 ^oC which is kept constant within $\pm$ 1 ^oC. Sunlight entering the instrument is a major heat source: the power at the prefilter is about 15 W, but most of the light is reflected from the filter surface back to the telescope. All motors of the instrument are switched off after completion of the setup to prevent additional warming. The wavelength stability of TESOS is determined by the stability of the spacings of the two FPIs. Plate separation and parallelism of the interferometers are controlled by a closed loop servo system. Despite this servo control, there are residual drifts of the effective plate separation leading to wavelength instabilities. These drifts result from changes of the dielectric constant of the air (due to changes of temperature, pressure and humidity), thermal effects of the capacitor

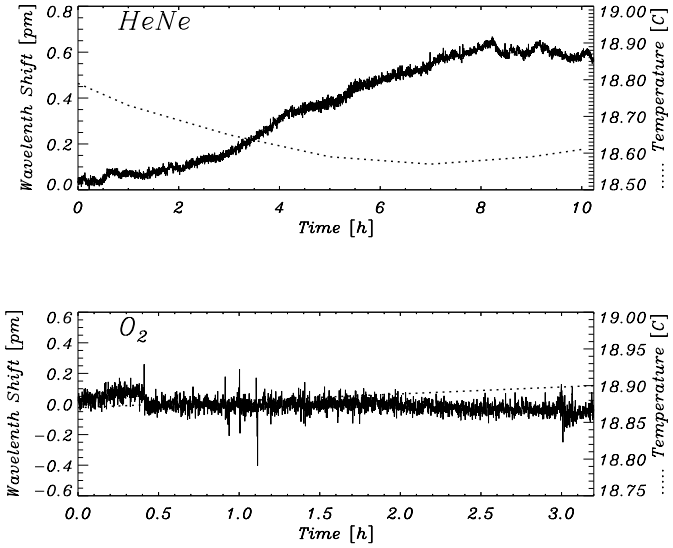

Fig. 10. Wavelength stability of TESOS. Upper panel: Night time measurement with an HeNe laser. Lower panel: Measurement of the telluric O_2 line (630.1 nm) during solar observation. The dotted line shows the temperature inside the instrument.

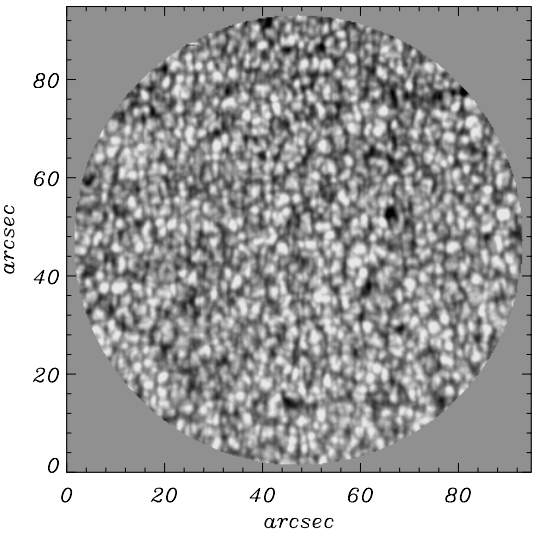

Fig. 11. Broadband continuum image (630 nm), average of 9 single frames (one line scan). Data of Figs. 11 and 12 have been taken on 2 July 1997.

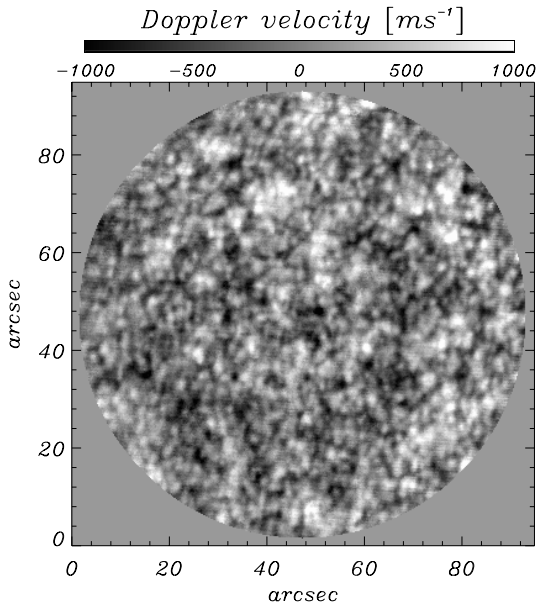

Fig. 12. Doppler map obtained from single scan (9 wavelength positions, step width 2 pm) through the Fe I 569.1 nm line.

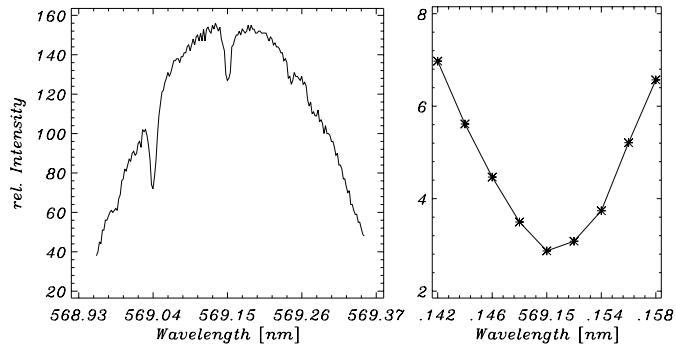

Fig. 13. Scan (using integrated light) through the full prefilter range around the Fe I 569.1 nm line (*left*) and the observed line profile averaged over the field of view of Fig. 12 (*right*).

elements and electronic drifts within the CS100 controller. The instrument stability was tested with long-time measurements using a HeNe laser and the telluric O_2 lines in the solar spectrum at 630.2 nm. Fig. 10 shows two examples of such measurements with the laser and with the O_2 line showing a wavelength drift between 1 and 1.3 pm/^oC. This leads to a typical ET50-FS stability of 0.1-0.3 pm/h during solar observations. These values are lower than the typical drifts of a grating spectrograph, but larger than in the Italian panoramic monochromator, a combination of an Universal Filter with a FPI (Cavallini 1997). They achieved a stability of 0.002 pm/h.

It should be noted that the stability values given in this section were achieved without a large effort. The wavelength drifts are small enough to allow for observing sequences with a duration of a few hours without re-tuning the instrument.

5.2. Solar observations

The examples shown in Figs. 11 to 15 are preliminary results from observations in July and December 1997. Data of the granulation image were taken at disk center in a quiet region using the magnetically insensitive line Fe I 569.1 nm with an integration time of 250 ms and a cycle time of 1.5 frames/s. The spectral scan consists of nine points and covers only the center of the line. Fig. 11 is the average of the 9 broadband continuum images taken simultaneously with the filtergrams. The rms intensity fluctuation of the averaged image is 3.3%. The Doppler map was obtained by fitting a polynomial to each observed profile. The rms-velocity is 370 m/s. The left panel of Fig. 13 shows the solar spectrum around the Fe I 569.1 nm line

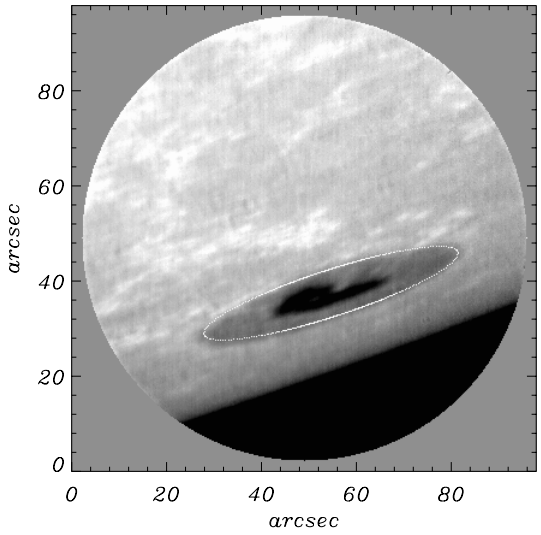

Fig. 14. Continuum image of a sunspot close to the solar limb. Observations were made in December 1997, integration time was 600 ms

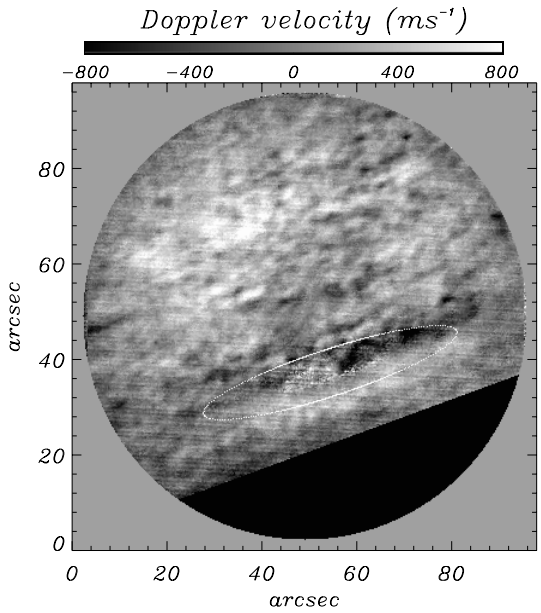

Fig. 15. Line-of-sight velocities of the sunspot image, derived from a single scan through the Fe I 557.6 nm line. The mean spot velocity is set to zero.

Table 4. TESOS characteristics

Spectral range	450–750 nm
Field of view	50/100 arcsec
Spectral resolution	320.000/160.000
Spatial scale	0.15/0.30 arcsec/pixel
Scan range	1 nm
Step width	$>$ 0.25 pm
Stability	$<$ 0.3 pm/h
SNR	500 (@250 ms)
Frame rate	1–2 frames/sec (typical)
Prefilters	FWHM 0.3 nm (4 filters)
Prefilter adjustment	+0/-0.2 nm
Detector	1024 x 1024 CCD (TH7896)
Pixel size	19 μm
Resolution	10 bit
FPI	Queensgate ET50-FS
User interface	SUN SPARC20
Motor Controller	CAN-BUS

measured through the prefilter with an FWHM of 0.3 nm.. The central part of the line and the wavelength scan positions are displayed in the right part of Fig. 13. Figs. 14 and 15 show the continuum and the line-of-sight velocity of a sunspot very close to the solar limb. Velocity values are given relative to the mean velocity of the spot. With 11 wavelength positions per scan and an integration time of 600 ms and a frame rate of 0.9 Hz one spectral scan was completed in about 12 s.

6. Summary

First observations and the test results shown in the previous section demonstrate that TESOS is a versatile device which meets most of its design goals. The main characteristics of TESOS are summarized in Table 4. There are still a few improvements to be made that we hope to implement in the near future. One drawback is the frame rate of 1–2 Hz, caused by the integration and readout time. The integration time can be reduced at the cost of decreased SNR, readout and storage rates are properties of the presently installed hard- and software. All mirrors within TESOS (and of the correlation tracker) are presently being coated with silver, which will increase the total transmission (telescope + correlation tracker + spectrometer) by about a factor of two and thus reduce the necessary integration time for a given signal-to-noise ratio. Other modifications include the installation of faster storage devices and some improvements of the camera software. The upgrade to a triple etalon system remains a long-term goal.

Acknowledgements. We would like to thank the members of the mechanical and electronic workshops of the KIS for their work in manufacturing TESOS. The camera driver was written by Fritz Stauffer at NSO. Libsx is a share-ware library written by Dominic Giamapolo (dbg@sgi.com). One of us (M.S.) is supported by the Deutsche Forschungsgemeinschaft under grant Schm1168/1-2.

References

Atherton P.D., Taylor K., Pike C.D. et al., 1982, MNRAS, 201, 661
Bendlin C., Volkmer R., Kneer F.: 1992, A&A 257, 817
Cavallini F., 1997, submitted to A&A
Darvann T., Owner-Petersen M., 1994, LEST Technical Report 57
Etschberger, K., 1994, "CAN Controller Area Network", Hanser Verlag, ISBN 3-446-17596-2
Gehrke E., Von Baeyer, P., 1906, Ann. Phys.(Leipzig), 20, 269
Houston W.V., 1927, Phys. Rev., 29, 478
Loughhead R.E., Bray R.J., Brown N.: 1978, Appl. Opt. 17, 3, 415
Mack J.E., McNutt D.P., Roesler F.L. and Chabbal R., 1963 Appl. Opt., 2, 873
McNutt, D.P., 1965, J. Opt. Soc. Am., 55, 288

Stoner J.P., 1966, J. Opt. Soc. Am., 56, 370
Ramsay J.V., Kobler H., Mugridge E.G.V., 1970, Solar Phys., 12, 492
Schlichenmaier R., Jahn K., Schmidt H.U., 1998, AJ 493, L121
Schmidt W., 1998, Proc. HRSAD Workshop, J. Bookbinder and E. DeLuca, Eds., 1998, in press
Tritschler A., Schmidt W., Knölker M., ASP-conference series 118, B. Schmieder et al. Eds., 170 (1997)
Schmidt W., Kentischer T.J., 1995 A&AS, 113, 363
v. Uexküll M., Kneer F., 1995, A&A 294, 252
Vaughan, J.M., 1989, "The Fabry-Perot Interferometer, History, Theory, Practice and Applications", The Adam Hilger Series on Optics and Optoelectronics
Westendorp Plaza C., del Toro Iniesta J.C., Ruiz Cobo B. et al., 1997, Nature 389, 47
Young E.R. and Clark K.C., 1980, Appl. Opt.,19, No 15, 2631